Diffraction of plane waves by finite-radius spiral phase plates of integer and fractional topological charge

Hipolito Garcia-Gracia and Julio C. Gutiérrez-Vega*

Photonics and Mathematical Optics Group, Tecnológico de Monterrey, Monterrey, México, 64849
**Corresponding author: juliocesar@itesm.mx*

Received September 30, 2008; revised January 30, 2008; accepted February 4, 2009;
posted February 4, 2009 (Doc. ID 102218); published March 17, 2009

A detailed analysis of the plane-wave diffraction by a finite-radius circular spiral phase plate (SPP) with integer and fractional topological charge and with variable transmission coefficients inside and outside of the plate edge is presented. We characterize the effect of varying the transmission coefficients and the parameters of the SPP on the propagated field. The vortex structure for integer and fractional phase step of the SPPs with and without phase apodization at the plate edge is also analyzed. The consideration of the interference between the light crossing the SPP and the light that undergoes no phase alteration at the aperture plane reveals new and interesting phenomena associated to this classical problem. © 2009 Optical Society of America

OCIS codes: 050.1970, 050.4865, 260.1960.

1. INTRODUCTION

The old problem of plane-wave diffraction by a circular aperture or an obstacle is classic in optics [1,2] and, surprisingly even nowadays, receives considerable attention by researchers [3–8]. The development of new approaches and numerical tools allows one to refine the existing solutions or provide alternative ones enriching the physical understanding of this classic problem. On the other hand, the study of screw-dislocated light waves caused by spiral phase plates (SPPs) has gained increasing interest in the past few years [9–14]. Research into light diffraction by SPPs is relevant in connection with optical micromanipulation, transfer of orbital angular momentum, and quantum information studies, among other important applications. Most of the studies have focused on the diffraction produced by infinite-extent SPPs with integer or fractional topological charges with various types of illumination. As far as we know, the problem of finding the diffraction of plane and Gaussian waves by hard-apertured SPPs was first addressed by Kotlyar *et al.* in [15,16]. Assuming zero light transmission outside of the SPP, they derived analytical expressions for the Fresnel and Fraunhofer diffraction patterns in terms of series of hypergeometric functions. In a more realistic situation, where the extent of the incident wave can be several times larger than the finite diameter of the SPP, the consideration of the interference between the light crossing the SPP and the light that undergoes no phase alteration at the aperture plane can be of crucial importance.

In this paper we study the general problem of plane-wave diffraction by a finite-radius circular SPP with integer and fractional topological charge and with variable transmission coefficients inside and outside of the plate edge. We characterize the effect of varying the transmission coefficients and the parameters of the SPP on the propagated field. Particular emphasis is made on the vortex structure and the total vortex strength of the diffracted wavefronts during the continuous transition from n to $n+1$ topological charge of the SPP. We corroborated that the interference between the light diffracted by the SPP and the light that undergoes no phase alteration at the aperture plane not only modifies the symmetry properties of the diffracted pattern, but also its optical vortex structure. The effects of a phase apodization at the SPP edge on the field distribution and its vortex structure are studied in detail as well. The appropriate form of Babinet's principle for the problem is presented and numerically confirmed. This work extends and consolidates previous studies on the diffraction of SPPs, and generalizes several known special cases, for example, the hard circular aperture and obstacle [1,2,4,5], the uniform-phase disk, and the infinite and finite-radius SPP [12,15,16], among others.

2. STATEMENT OF THE PROBLEM

The general problem is formulated as follows: a linearly polarized plane wave with wave number k, time dependence $\exp(-i\omega t)$ illuminates a circular SPP with radius a and topological charge α (Fig. 1). The wave field at the initial plane $(r_0, \varphi_0, z=0^+)$ is

$$U(r_0,\varphi_0)=\begin{cases} A_1\exp(i\alpha\varphi_0+i\beta) & r_0\leq a \\ A_2 & r_0>a \end{cases}, \qquad (1)$$

where the transmission coefficients A_1 and A_2 are complex in the most general situation $(0\leq|A_1|, |A_2|\leq 1)$, α defines the phase singularity of strength $2\pi\alpha$, and β introduces an optional uniform phase shift on the light that passes through the SPP. The possibility of adjusting the four parameters $(A_1, A_2, \alpha, \beta)$ allows one to model a variety of special cases, including, for example, a transparent

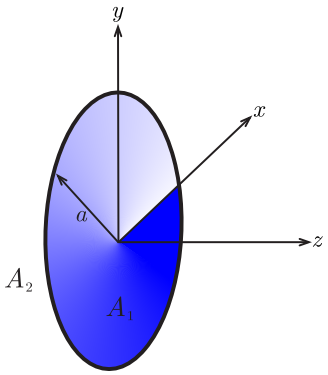

Fig. 1. (Color online) Geometry of the SPP aperture function.

aperture ($A_1=1$, $A_2=0$, $\alpha=0$, $\beta=0$), a hard-apertured finite-radius SPP of integer order ($A_1=1$, $A_2=0$, $\alpha=n$, $\beta=0$), or a transparent uniform-phase plate ($A_1=1$, $A_2=0$, $\alpha=0$, β). Throughout this paper we assume that the aperture diameter is much larger than the wavelength (i.e., $ka \gg 1$).

A. Fresnel Diffraction

In the paraxial approximation, the complex amplitude $U(\mathbf{r})$ at the observation point $\mathbf{r}=(r,\varphi,z)$ can be obtained with the Huygens–Fresnel integral [17],

$$U(\mathbf{r}) = -\frac{ik}{2\pi z}\exp\left(i\frac{kr^2}{2z}\right)\int_0^\infty r_0 dr_0 \int_0^{2\pi} d\varphi_0 U(r_0,\varphi_0) \times \exp\left\{i\frac{k}{2z}[r_0^2 - 2rr_0\cos(\varphi_0-\varphi)]\right\}, \quad (2)$$

where $U(r_0,\varphi_0)$ is the aperture function of the diffracting object located at the $z=0$ plane. When the aperture function contains either amplitude or phase discontinuities, Eq. (2) is only valid for distances

$$z \geqslant L = 2a(ka/\pi)^{1/3}, \quad (3)$$

where a is the distance from the propagation axis to the farthest discontinuity [17]. In Sections 3 and 4 we will solve the Huygens–Fresnel integral for several meaningful and unexplored cases of the general transmittance Eq. (1).

B. Fraunhofer Diffraction

In the region of Fraunhofer diffraction (i.e., the far field), the Huygens–Fresnel integral Eq. (2) simplifies to

$$U_{\text{far field}}(\mathbf{r}) = \frac{k}{i2\pi z}\exp\left(i\frac{kr^2}{2z}\right)\int_0^\infty r_0 dr_0 \int_0^{2\pi} d\varphi_0 U(r_0,\varphi_0) \times \exp\left[-i\frac{krr_0}{z}\cos(\varphi_0-\varphi)\right]. \quad (4)$$

For the initial field Eq. (1), the Fraunhofer diffraction integral Eq. (4) can be analytically evaluated yielding the following result:

$$U_{\text{far field}}(\mathbf{r}) = \frac{ka^2}{iz}\exp\left(i\frac{kr^2}{2z}\right)\left\{A_1\frac{(-i)^n\exp(in\varphi)}{(n+2)\Gamma(n+1)}\left(\frac{\rho}{2}\right)^n \times {}_1F_2\left(1+\frac{n}{2},2+\frac{n}{2},1+n;-\frac{\rho^2}{4}\right) + A_2\left[\delta(\rho)-\frac{J_1(\rho)}{\rho}\right]\right\}, \quad (5)$$

where $\rho \equiv kar/z$ is the normalized radius, $\Gamma(x)$ is the gamma function, $J_1(x)$ is the first-order Bessel function, δ is the Dirac delta function, and ${}_1F_2(\alpha,\beta,\gamma;x)$ is the hypergeometric function

$${}_1F_2(\alpha,\beta,\gamma;x) = \sum_{m=0}^{\infty}\frac{(\alpha)_m}{(\beta)_m(\gamma)_m m!}x^m, \quad (6)$$

with $(\alpha)_m \equiv \Gamma(\alpha+m)/\Gamma(\alpha)$ being the Pochhammer symbol. The first summand of Eq. (5) represents the contribution of the light crossing through the SPP and has been reported previously in some works, e.g., Eq. (3) in [15]. On the other hand, the second summand of Eq. (5) represents the contribution of the light crossing the aperture plane outside of the SPP, and actually corresponds to the diffraction of a plane wave by a circular opaque obstruction.

Two observations are in order: first, Eq. (1) assumes the infinite extent of the incident plane wave. It should be noted that such an assumption is not always realistic, being conventionally used in analytical calculations, whereas upon numerical simulation the use of a limiting aperture is inevitable. Additionally, Eq. (1) assumes an ideal aperture such that the wave field is discontinuous at the boundary $r_0=a$ in the most general situation. The consequences of these two assumptions will be discussed later in Section 3.

3. FINITE-RADIUS INTEGER-STEP SPIRAL PHASE PLATE

Let us first consider the case when the phase step of the SPP is integer, i.e., $\alpha=n$. By substituting the initial field Eq. (1) into the Huygens–Fresnel integral Eq. (2), separating the radial integral, and solving the angular integral with the help of the known result

$$\int_0^{2\pi} d\varphi_0 \exp\left[-i\frac{kr}{z}r_0\cos(\varphi_0-\varphi)+in\varphi_0\right] = i^n 2\pi\exp(in\varphi)J_n\left(-\frac{kr}{z}r_0\right), \quad (7)$$

where J_n is an nth-order Bessel function, we obtain the diffraction pattern of a finite-radius integer-step SPP, namely

$$U_n(r,\varphi;z) = -\frac{ika^2}{z}\exp\left(i\frac{kr^2}{2z}\right) \times [A_1(-i)^n\exp(in\varphi+i\beta)G_n(r,z) - A_2G_0(r,z)] + A_2, \quad (8)$$

where

$$G_n(r,z) = \int_0^1 w \exp\left(i\frac{ka^2}{2z}w^2\right) J_n\left(\frac{kar}{z}w\right) \mathrm{d}w, \qquad (9)$$

and $G_0(r,z)$ in Eq. (8) is a special case of Eq. (9) for $n=0$.

For arbitrary values of its parameters, it appears that the integral in Eq. (9) cannot be evaluated in closed form. In view of this, Kotlyar *et al.* [15] derived the following series expression for $G_n(r,z)$ in terms of hypergeometric functions:

$$G_n(r,z) = \frac{1}{n!}\left(\frac{ikar}{2z}\right)^n \sum_{m=0}^{\infty} \frac{1}{(2m+n+2)m!} \times \left(\frac{ika^2}{2z}\right)^m {}_1F_2\left[\frac{2+2m+n}{2}, \frac{4+2m+n}{2}, 1+n; -\left(\frac{kar}{2z}\right)^2\right]. \qquad (10)$$

Even though Eq. (10) is an exact series solution of Eq. (9), from a numerical point of view its evaluation can be cumbersome, especially for small propagation distances (of the order of L) for which the factor $(ka^2/2z)^m$ increases dramatically.

The application of the standard numerical integration methods, e.g., Gaussian–Legendre quadrature, to evaluate Eq. (9) is also not practical because the integrand can be highly oscillatory depending of the magnitude of the term k/z inside both the exponential and the argument of the Bessel function. To save this crucial point, in this paper we will employ the partitioned Gaussian quadrature method (PGQM) introduced originally by Haider and Liu [18] to numerically calculate Fourier and Bessel transforms of highly oscillatory functions, and that, in our numerical tests, resulted to be the more accurate and reliable method to evaluate $G_n(r,z)$ and $G_0(r,z)$.

A. Uniform-Phase Disk ($n=0$, $\beta\neq 0$)

A disk of radius a with uniform phase shift β and variable transmission coefficients can be easily modeled with Eqs. (1) and (8) by setting $n=0$ and $\beta\neq 0$. Depending on the selected values of A_1, A_2, and β, we can model different physical setups, such as a circular aperture ($A_1=1$, $\beta=0$) in a completely opaque plane $A_2=0$, or an opaque circular obstacle ($A_1=0$, $A_2=1$, $\beta=0$), or a transparent plane $A_2=1$ and a transparent circular disk $A_1=1$ with arbitrary phase shift β.

Figure 2 shows the radial distribution of the intensity and phase of the diffracted plane waves by three different physical versions of the disk with phase shift $\beta=\pi/5$: a disk with unitary transmission coefficients $A_1=A_2=1$, a disk with $A_1=0.8$ and $A_2=0.4$, and a disk with interchanged transmission coefficients, i.e., $A_1=0.4$ and $A_2=0.8$. All diffraction patterns throughout this document where calculated using plane waves of $\lambda=632.8$ nm and phase objects of radius $a=500$ μm. We can see from Fig. 2 that when the inner transmission coefficient A_1 has a bigger value than the outer transmission coefficient A_2, the main characteristic in the intensity distribution is a difference in the constant levels of its oscillatory behavior, whereas the phase distribution presents a phase-jump structure located exactly at the position of the discontinuity $r/a=1$. Both the magnitude of the phase jump and the amplitude of the oscillations in the $r/a>1$ region increase as $A_2\to 0$ [Fig. 3(a)].

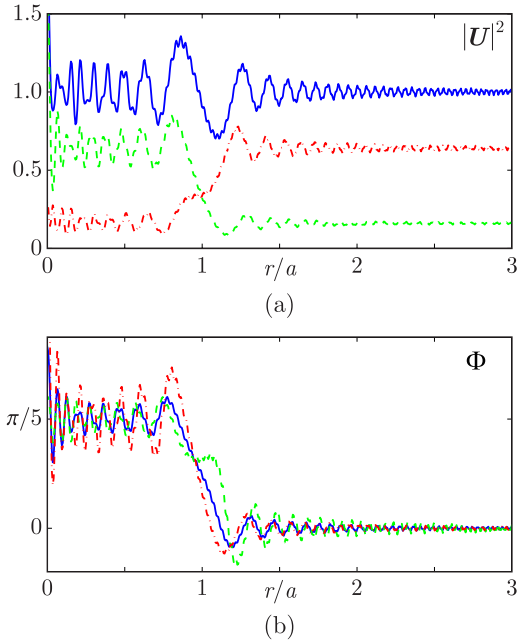

Fig. 2. (Color online) (a) Intensity and (b) phase of diffracted plane waves by uniform-phase disks of $\beta=\pi/5$ with $A_1=1$ and $A_2=1$ (solid curve), with $A_1=0.8$ and $A_2=0.4$ (dashed curve), and with $A_1=0.4$ and $A_2=0.8$ (dashed-dotted curve), observed at $z/L=2$.

On the other hand, when the inner transmission coefficient A_1 is smaller than the outer transmission coefficient

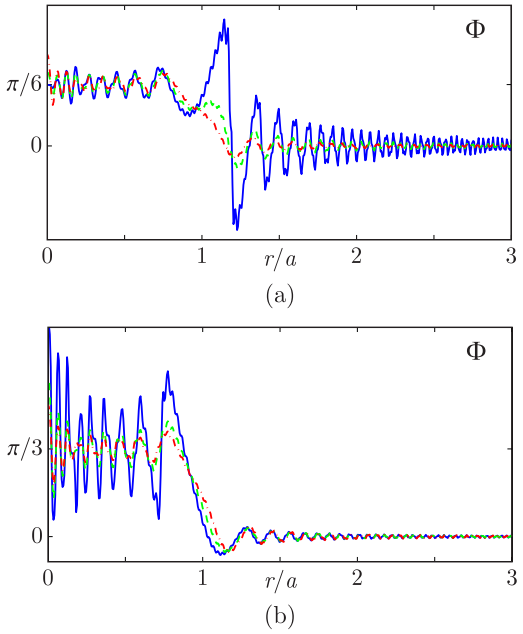

Fig. 3. (Color online) Radial phase distributions of the diffraction patterns at $z/L=2$ caused by disks with (a) phase shift $\beta=\pi/6$, inner transmission coefficient $A_1=1$, and outer transmission coefficients $A_2=0.2$ (solid curve), 0.5 (dashed curve), and 0.8 (dashed-dotted curve); (b) phase shift $\beta=\pi/3$, outer transmission coefficient $A_2=0.9$, and inner transmission coefficients $A_1=0.2$ (solid curve), 0.5 (dashed curve), and 0.8 (dashed-dotted curve).

A_2 there is no significant perturbation in the radial phase distribution at $r/a=1$, but the amplitude of the oscillations in the shadow of the disk, i.e., $r/a<1$ increases as $A_1 \to 0$. This behavior can be seen in Fig. 3(b).

B. Babinet's Principle

The fact that the transmission coefficients were left as free parameters allowed us to confirm Babinet's principle, which, in our case, takes a different form than the one usually found in textbooks [1]. Let U_{A_1,A_2} be the diffraction pattern due to a plane wave passing through a uniform-phase disk with transmission coefficients A_1, A_2, and phase shift β. For complementary screens U_{A_1,A_2} and $U_{1-A_1,1-A_2}$, and real-valued transmission coefficients $0 \leqslant A_1, A_2 \leqslant 1$, Babinet's principle can be rewritten as

$$U_{A_1,A_2} + U_{1-A_1,1-A_2} = U_{1,1}. \tag{11}$$

Equation (11) also holds when the values of the transmission coefficients themselves are complementary, that is $A_1+A_2=1$. However, if instead of complementing each transmission coefficient we invert them, the expression for the alternate form of Babinet's principle changes, too, and is given by

$$U_{A_1,A_2} + U_{A_2,A_1} = (A_1 + A_2)U_{1,1}. \tag{12}$$

The numerical confirmation of Eq. (12) is shown in Fig. 4, where we see that there is very good agreement between $(A_1+A_2)U_{1,1}$ and $U_{A_1,A_2}+U_{A_2,A_1}$ radial diffraction patterns, both for the intensity and phase distributions.

C. Integer-Step Spiral Phase Plate ($n \neq 0$, $\beta=0$)

The diffraction pattern caused by a finite-radius SPP of integer topological charge $\alpha=n$ can be obtained from Eq. (8) by setting $\beta=0$. In Fig. 5 we show the transverse intensity and phase distributions of the Fresnel diffraction patterns caused by SPPs of charge $n=1$, observed at three different propagation distances $z/L=\{1.0, 2.5, 4.0\}$. As both Kotlyar *et al.* [15] and Berry [12] showed previously, the intensity of the diffraction pattern caused by infinite SPPs of integer charge exhibits azimuthal symmetry. However, due to the interference between the light that passes through the SPP and the light that undergoes no phase alteration, the intensity distribution no longer exhibits azimuthal symmetry. Furthermore, it is possible to see in Fig. 5 that as the diffracted plane wave propagates away from the aperture plane, the topological characteristics in the intensity distribution suffer from broadening and coarsening processes. These coarsening processes can be easily appreciated by comparing Figs. 5(a) and 5(c), as we can see that the number of ripples between the origin and the low intensity region located at the border of the SPP diminishes considerably, and the ripples that remain are wider and more pronounced than the ones observed at the closest observation distance.

On the other hand, as Berry showed in [12], the transverse phase distribution of the diffraction pattern caused by an nth order SPP presents n discontinuity lines symmetrically distributed every $2\pi/n$ rad, each with its own oscillatory decoration. However, different to that discussed by Berry [12], when the SPP has a finite radius a and there is light that suffers no phase perturbation, the discontinuity lines become finite and spread from the origin of the SPP up to its border at $r/a=1$, instead of having infinite extent as would be expected for an infinite SPP, which can be observed in the right column of Fig. 5.

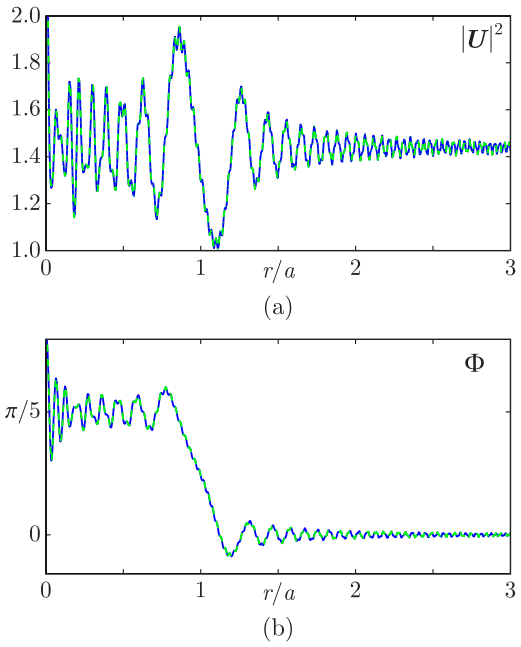

Fig. 4. (Color online) Comparison between (a) intensity and (b) phase of $(A_1+A_2)U_{1,1}$ (solid curve) and $U_{A_1,A_2}+U_{A_2,A_1}$ (dashed curve) for $A_1=0.8$, $A_2=0.4$ and $\beta=\pi/5$, observed at $z/L=2$.

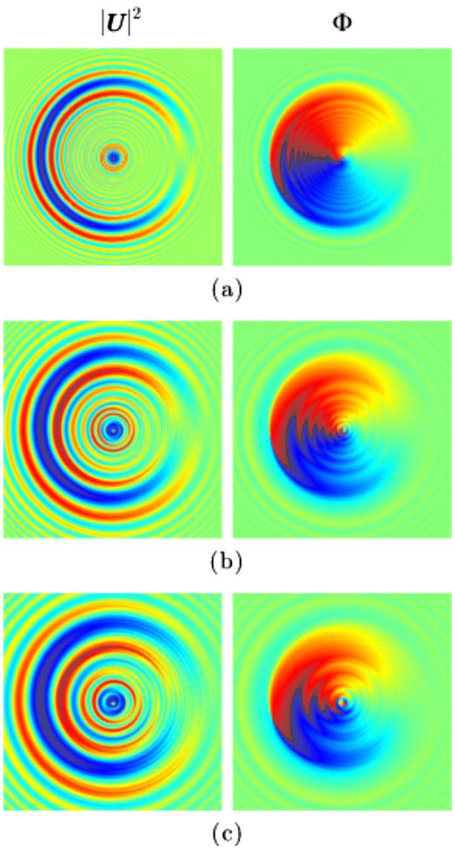

Fig. 5. (Color online) Intensity and phase distributions of the diffraction pattern caused by a $n=1$ finite-radius SPP, observed on $3a \times 3a$ windows at $z/L=$(a) 1.0, (b) 2.5, and (c) 4.0.

In [15] Kotlyar *et al.* presented the intensity distribution of the diffraction pattern caused by a SPP with $n=3$ illuminated by a finite-radius plane wave. The physical setup used by Kotlyar *et al.* [15] can be modeled by setting the transmission coefficients to $A_1=1$ and $A_2=0$, which is shown in Fig. 6(a). However, Eq. (1) allows us to change the transmission coefficients and Eq. (8) provides the Fresnel diffraction pattern for any values of A_1 and A_2. Taking advantage of this, in Fig. 6 we can see how the intensity and phase distributions of the Fresnel diffraction pattern change as A_2 goes from 0 to 1; note the loss of azimuthal symmetry in the intensity distribution and the spiral behavior of the discontinuity lines in the illuminated region $r>a$ of the phase distribution. It is also possible to observe in the left column of Fig. 6 that once $A_2 \neq 0$, there no longer exists a $n=3$ vortex on the propagation axis, since as $A_2 \to 1$ a nonzero intensity spot appears at the origin.

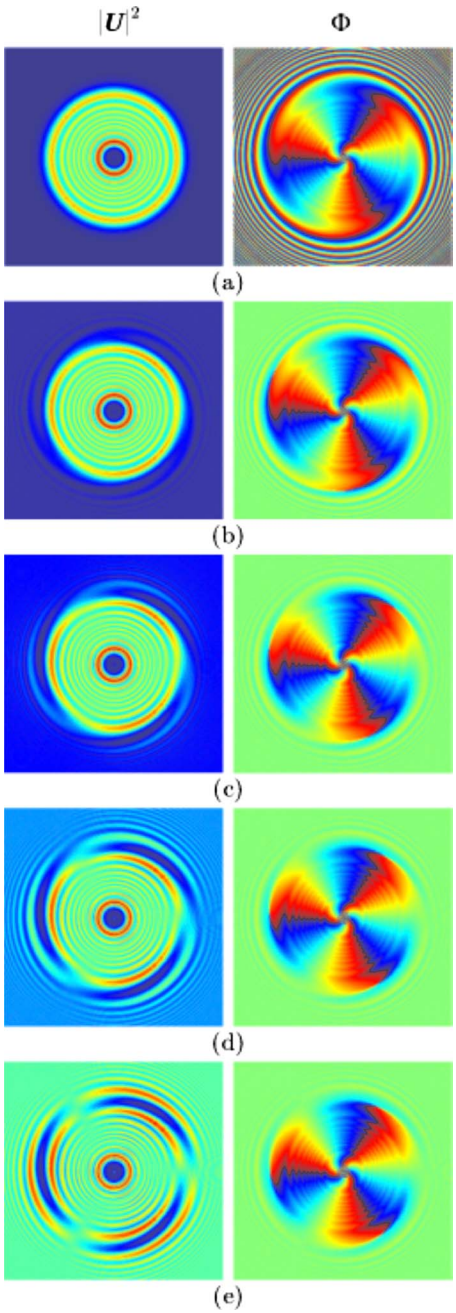

Fig. 6. (Color online) Intensity and phase distributions of the diffraction pattern caused by a $n=3$ finite-radius SPP, observed at $z/L=1.0$ for $A_1=1$ and $A_2=$(a) 0, (b) 0.25, (c) 0.5, (d) 0.75, and (e) 1.

D. Optical Vortex Structure of the Integer-Step Spiral Phase Plate

The vortex strength S_n of a light distribution inside the transverse circuit C is determined with the line integral

$$S_n = \frac{1}{2\pi}\oint_C \mathrm{d}\varphi \frac{\partial \Phi(\mathbf{r})}{\partial \varphi}, \tag{13}$$

where $\Phi(\mathbf{r})$ is the phase distribution of the wave field, and C is a closed non-self-intersecting loop directed in the positive (anticlockwise) sense in the transverse plane, not passing through any vortex.

At the initial plane $z=0$, if C encloses the aperture in Eq. (1) the total vortex strength is $S_n=0$ independent of the value of A_2 and n. Since an n-strength vortex is located at the origin, then a topological charge of $-n$ should be contained somehow in the boundary of the aperture at $r_0=a$. The distribution of this negative charge along the boundary is indeterminate because Eq. (1) assumes an ideal aperture whose transmittance is discontinuous at the boundary $r_0=a$ and, rigorously speaking, such an assumption is not physically realistic. In the presence of boundaries where the wave field changes abruptly isolated singularities may be created or destroyed at the boundary. To make explicit the position of the n negative vortices at the boundary one should rewrite the transmittance in Eq. (1) by inserting a thin transition region between the aperture and the plane wave such that the field and its gradient are everywhere continuous through the transverse plane. We will analyze this apodized scheme in more detail in Subsection 3.E.

Outside the initial plane, the interference between the light diffracted by the SPP and the light that undergoes no phase alteration at the aperture plane not only modifies the symmetry elements of the diffraction pattern, but also its optical vortex structure. In particular, the presence of light outside of the SPP border, i.e., $A_2>0$, leads to the appearance of n negative vortices at the periphery of the border of the SPP. Furthermore, on propagation, the axial n-strength vortex splits into a variable number of unit-strength vortices, none of which is located on the propagation axis, but all of them lie in its vicinity. These situations are shown in Fig. 7 for SPPs with $n=1$ and 2.

In free space propagation the phase singularities of a wave field can only be created or destroyed in such a way that the total topological charge is conserved. This means that, as the diffracted field propagates farther away from the aperture plane, vortices are created or annihilated in pairs with charges that have opposite signs but equal magnitudes, conserving the total topological charge $S_n=0$. This behavior can be observed in Fig. 8, where we show the intensity and phase distribution of the patterns caused by a transparent unit-charge SPP at four different propagation distances. Since the optical vortices near the propagation axis for $z/L=1.0$ are too close to the origin, a

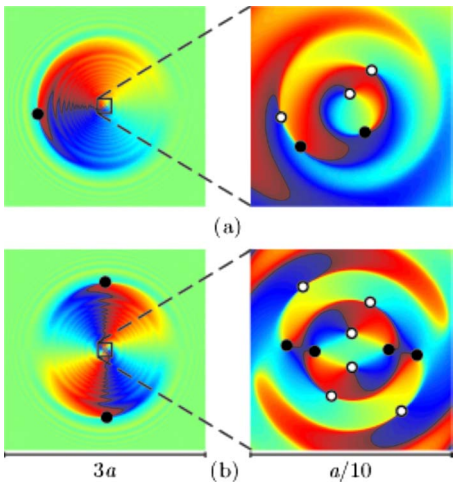

Fig. 7. (Color online) Location of vortices in the phase distribution of the diffraction pattern caused by a transparent finite-radius SPP, observed at $z/L=1.0$ for $n=$(a) 1 and (b) 2. Positive and negative vortices are represented by white and black small circles, respectively.

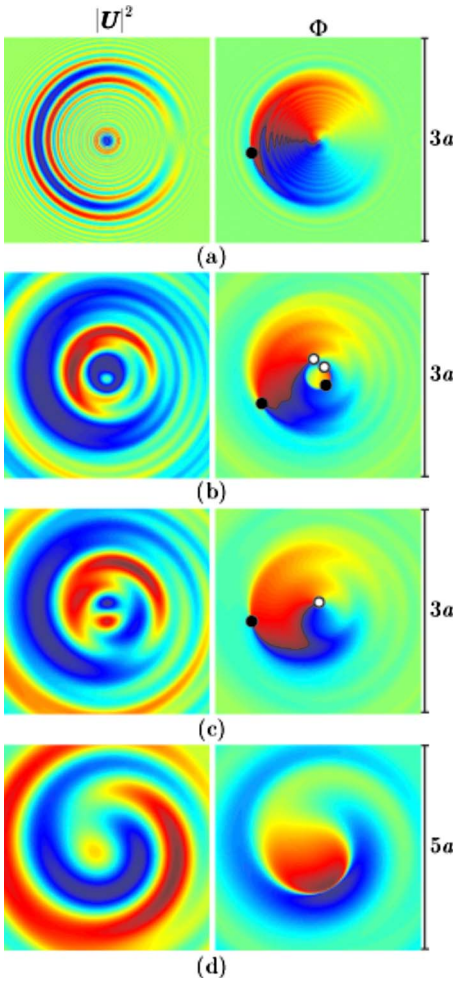

Fig. 8. (Color online) Intensity and phase distribution of the diffraction pattern caused by a transparent $n=1$ finite-radius SPP observed at $z/L=$(a) 1.0, (b) 15, (c) 25, and (d) 110 for $A_2=1$. Positive and negative vortices are represented by white and black small circles, respectively. A zoom of the central region of the phase in (a) is included in Fig. 7(a).

zoom of the central region is included in Fig. 7(a). The optical vortices in the diffraction patterns were numerically localized on the plane (x,y) using a simple routine which obtains the contour lines for $\mathrm{Re}\{U\}=0$ and $\mathrm{Im}\{U\}=0$ and finds the points of intersection between them.

E. Integer-Step Spiral Phase Plate With Phase Apodization

To study the plane-wave diffraction caused by the finite-radius integer-step SPP in a more realistic way, we modified the aperture function to include phase apodization at the border of the SPP. This phase-apodized version of the finite-radius SPP is defined as an extension of the one with unitary transmission coefficients, and its aperture function can be written as

$$U(r_0,\varphi_0)=\exp[in\varphi_0 f(r_0)]. \tag{14}$$

The apodization function $f(r_0)$ is given by

$$f(r_0)=\begin{cases}1 & r_0\leq a\\ \cos\left[\dfrac{\pi}{2\epsilon}(r_0-a)\right] & a<r_0\leq a+\epsilon,\\ 0 & r_0>a+\epsilon\end{cases} \tag{15}$$

where a is the radius of the SPP and ϵ is the apodization distance.

1. Changes in the Diffraction Pattern

The apodization introduced by $f(r_0)$ has a visible effect in the intensity distribution of the Fresnel diffraction pattern, as it loses its $2\pi/n$ rotation symmetry, gains azimuthal symmetry near the propagation axis, and acquires a spirallike behavior near the border of the phase plate, as can be seen in the left column of Fig. 9. The phase distribution of the diffraction pattern also suffers some changes, as the amplitude of the oscillatory decorations of the phase discontinuity lines diminishes as ϵ increases, and in the apodization region the discontinuity lines spiral around the SPP ending at the $+x$ axis, which can be observed in the right column of Fig. 9.

2. Optical Vortex Structure

The introduction of the apodization into the aperture function has some important consequences in the vortex structure of the diffraction pattern caused by the SPP. The apodization function has been chosen such that the field and its gradient are continuous everywhere through the transverse plane. In this way, the appearance of the negative vortices in the periphery of the SPP boundary is clear at the initial plane $z=0$. As expected, if the contour C in Eq. (13) encloses the aperture including the apodization region, the total vortex strength is $S_n=0$.

In Fig. 9 it is possible to appreciate that as the apodization distance increases, the central spot of nonzero intensity disappears as the optical vortices move closer to the propagation axis. Thus, it would be possible to assume that as $\epsilon\to\infty$, all the unit-strength vortices would merge at the origin and instead of having multiple unit-strength vortices, we would have a unique vortex of strength n, similar to the one generated by an infinite SPP, and its total vortex strength S_n would take the value correspond-

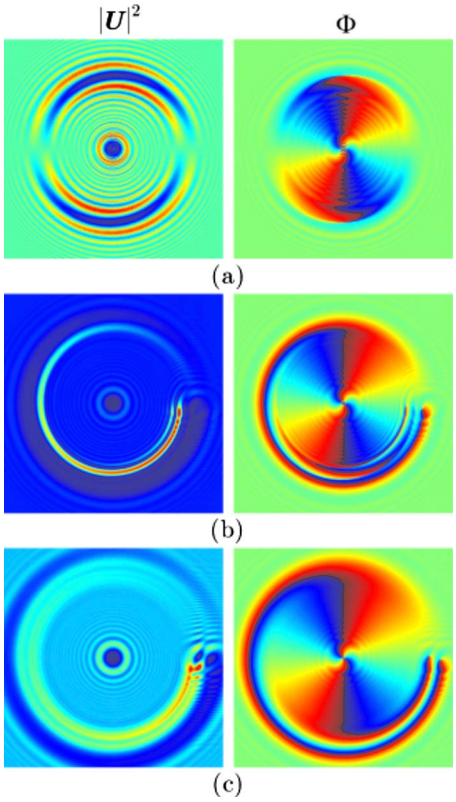

Fig. 9. (Color online) Intensity and phase distribution of the diffraction pattern caused by a $n=2$ finite-radius SPP observed at $z/L=1.0$, for apodization distances of $\epsilon=$(a) 0, (b) $0.25a$, and (c) $0.5a$.

ing to the topological charge of the SPP since the border vortices would not exist. However, due to the finite nature of the apodization distance, there are multiple unit-strength vortices around the propagation axis. Furthermore, it can be seen in Fig. 9 that the border vortices are no longer on opposite positions along the border of the SPP. Instead they are located at the $+x$ axis within the apodization region. On the other hand, the number of unit-strength vortices around the propagation axis is not the same for all nonzero values of the apodization distance, but it decreases as ϵ increases, which can be seen in the right column of Fig. 10.

The reduction in the number of vortices near the propagation axis, and the fact that those vortices are closer to the origin, both caused by the presence of a phase apodization beyond the border of the finite-radius integer-step SPP has another important consequence involving the "life length" of the vortex structure in the diffraction pattern. Since for larger values of the apodization distance ϵ the behavior of the diffracted wavefront approximately resembles that of an infinite SPP with finite-radius plane-wave illumination, it is not unexpected to observe that the vortex structure takes longer propagation distances to disappear from the diffraction pattern, although since $S_n=0$ it is bound to disappear for any finite value of ϵ. Thus, for larger values of ϵ, the optical vortices survive longer propagation distances, as can be seen in Fig. 11 where we show the maximum propagation distance occurred before the last vortex-pair annihilation event. The propagation distance in Fig. 11 is normalized

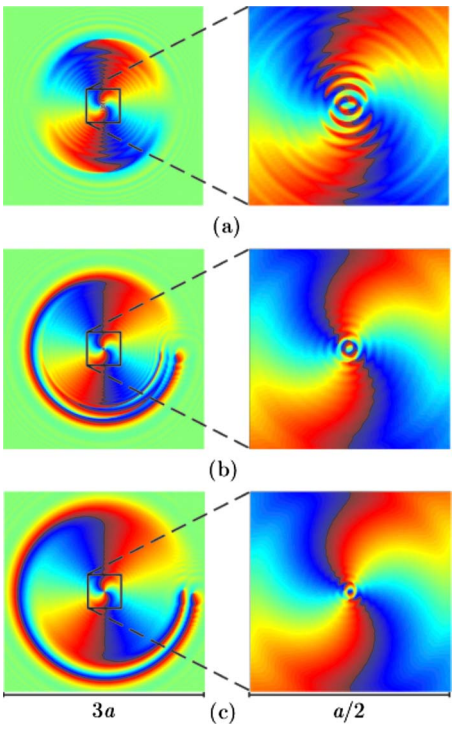

Fig. 10. (Color online) Phase distribution of the diffraction pattern caused by a $n=2$ finite-radius SPP observed at $z/L=1.0$, for apodization distances of $\epsilon=$(a) 0, (b) $0.25a$, and (c) $0.5a$.

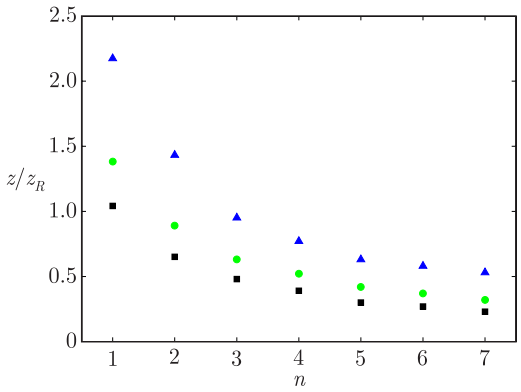

Fig. 11. (Color online) Propagation distance before the last vortex-pair annihilation event for different topological charges n and with apodization distances $\epsilon=0$ (squares), $0.2a$ (circles), and $0.5a$ (triangles).

against the Rayleigh distance given by $z_R=ka^2/2$. It is also possible to observe in Fig. 11 that the life length of the vortex structure falls asymptotically with the order n of the SPP. This is easy to explain, as a larger topological charge n translates into more vortices in the diffraction pattern, which in turn generates faster and more frequent interactions between the optical vortices, thus considerably diminishing the propagation distance they are capable of surviving.

4. FINITE-RADIUS FRACTIONAL-STEP SPIRAL PHASE PLATE

The general case of a SPP with fractional phase step α can be expressed in a manner very similar to that of the

integer-step analyzed previously, save for the constant phase shift β. The SPP has an arbitrary transmission coefficient A_1, and induces a phase shift $\exp(i\alpha\varphi_0)$ on the light that passes through it, for $\alpha \in \mathbb{R}$. The rest of the aperture plane presents a constant transmission coefficient A_2. This can be summarized in a simple mathematical expression given by

$$U(r_0,\varphi_0) = \begin{cases} A_1 \exp(i\alpha\varphi_0) & r_0 \leqslant a \\ A_2 & r_0 > a \end{cases}, \tag{16}$$

where a is the radius of the SPP. Since α is an arbitrary real number, the angular integral in Eq. (2) for $r \leqslant a$ has no closed form solution for arbitrary values of φ_0. To save this problem, we can carry out a complex Fourier series expansion of the term $\exp(i\alpha\varphi_0)$; from [19] we have

$$\exp(i\alpha\varphi_0) = \frac{(-1)^\alpha \sin(\alpha\pi)}{\pi} \sum_{m=-\infty}^{\infty} \frac{\exp(im\varphi_0)}{\alpha - m}. \tag{17}$$

By using Eq. (17), and carrying out the Huygens–Fresnel integral for each harmonic component, we obtain the following Fresnel diffraction pattern caused by a finite-radius SPP with fractional topological charge α when illuminated by an ideal plane wave:

$$U(r,\varphi;z) = A_2 - \frac{ika^2}{z} \exp\left(i\frac{k}{2z}r^2\right) \times \sum_{m=-\infty}^{\infty} C_m \exp(im\varphi) G_{|m|}(r,z), \tag{18}$$

where the expansion coefficients C_m are

$$C_m = A_1 \frac{(-1)^\alpha \sin(\alpha\pi)}{\pi} \frac{(-i)^{|m|}}{\alpha - m} - A_2\delta_{m,0}, \tag{19}$$

$G_{|m|}(r,z)$ is given by Eq. (9) replacing $n \to |m|$, and $\delta_{m,n}$ is the Kronecker delta symbol.

It is possible to see that Eq. (18) is in fact a general expression for the Fresnel diffraction pattern of a finite-radius SPP of arbitrary real topological charge α, since the case of integer topological charge n is also covered by it. To show that, the limit of the α-dependent term of expansion coefficients C_m when $\alpha \to n$ is observed,

$$\lim_{\alpha\to n}\left[\frac{(-1)^\alpha \sin(\alpha\pi)}{\pi(\alpha - m)}\right] = \begin{cases} 1 & \text{for } m = n \\ 0 & \text{for } m \neq n \end{cases}, \tag{20}$$

so it is possible to express C_m as

$$C_m|_{\alpha=n} = A_1(-i)^{|m|}\delta_{m,n} - A_2\delta_{m,0}. \tag{21}$$

We can see that substituting Eq. (21) into Eq. (18) yields the same expression as Eq. (8) for $n \geqslant 0$. For $n < 0$ it is just a matter of invoking the Bessel identity under sign change in the order.

The Fresnel diffraction pattern for a SPP of fractional topological charge α is quite different from the ones for integer charge n. This is due to the fact that, besides the phase singularity at the origin, there is a phase jump along the positive x axis due to the fractional nature of α. Because of this, the intensity of the diffraction pattern shows a spiral-like behavior similar to the one observed for integer topological charge, and an additional low intensity region along the $+x$ axis caused by the phase discontinuity present there. This behavior is similar to the one predicted by Berry in[12], with the main difference being that the pattern has a spiral-like nature and is finite due to the effect of the diffraction waves caused by the border of the SPP. As the topological charge α increases from n to $n+1$, a new dark spiral lobe gradually grows out from the end of the low intensity region, at $x = a$ (Fig. 12). This process continues until α approaches $n+1$, and the dark stripe diminishes its size as the additional spiral lobe is fully formed. In a similar fashion, as α increases from n to $n+1$ the phase distribution of the diffraction pattern gains an additional phase discontinuity line which grows out from the $+x$ axis.

A. Optical Vortex Structure

The vortex structure of the diffraction pattern caused by a fractional-step SPP changes as α goes from n to $n+1$. When $\alpha < n+1/2$, the phase distribution of the diffraction pattern has n vortices located at the border of the SPP, each one at the end of a phase discontinuity line, and a variable number of vortices near the propagation axis. On the other hand, when $\alpha > n+1/2$, the phase distribution shows $n+1$ border vortices, and their respective discontinuity lines, and more central vortices than the previous case. We can better appreciate this behavior of the diffraction pattern in Fig. 13.

However, the situation changes when α is a half integer, i.e., $\alpha = n+1/2$. When the topological charge of the SPP takes on a half integer value, a finite number of unit

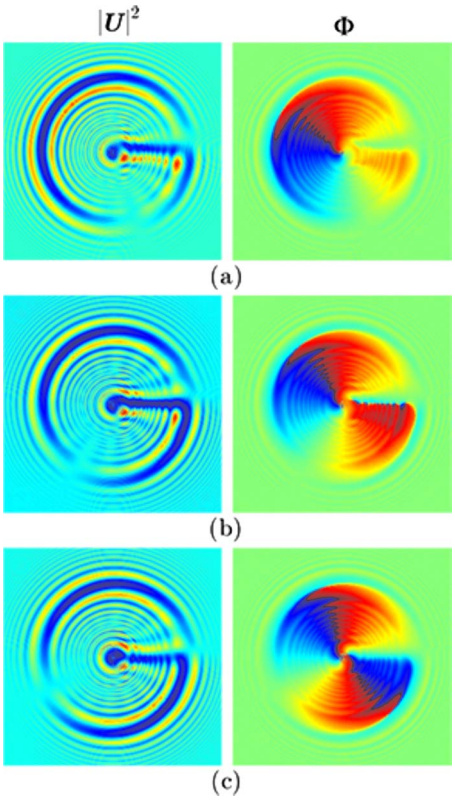

Fig. 12. (Color online) Intensity and phase of the diffraction pattern observed at $z/L = 1.0$, caused by a finite-radius SPP with fractional charges α=(a) 1.25, (b) 1.5, and (c) 1.75.

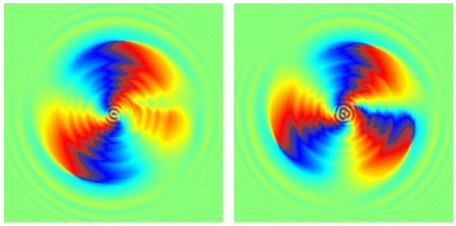

Fig. 13. (Color online) Phase distribution of the diffraction pattern observed at $z/L=2.0$, caused by a finite-radius SPP with fractional charges $\alpha=$(a) 2.3 and (b) 2.7.

strength vortices, alternating sign, appear on the $+x$ axis due to the birth of the $(n+1)$th phase discontinuity line (Fig. 14). As α grows beyond $n+1/2$, these vortices experience pair-annihilation processes that in the end leave an extra border vortex, and some additional central vortices, which accounts for the difference in the number of ± 1 vortices between the $\alpha<n+1/2$ and $\alpha>n+1/2$ diffraction patterns. However, despite the complicated behavior of the optical vortex structure for fractional topological charges, the total vortex strength remains $S_\alpha=0$ for all values of α.

B. Phase-Apodized Fractional-Step Spiral Phase Plate

As with the integer-step SPP, the more general situation of a phase-apodized fractional-step SPP is studied. The aperture function of the apodized version of the SPP with fractional topological charge α is given by

$$U(r_0,\varphi_0)=\exp[i\alpha\varphi_0 f(r_0)], \tag{22}$$

where $f(r_0)$ is given by Eq. (15).

The introduction of the phase-apodization function $f(r_0)$ into the aperture function of the fractional-step SPP has effects similar to the ones observed in the integer-step SPP. By comparing the left columns of Figs. 12 and 15, we can see that the intensity distribution of the diffraction pattern is no longer segmented into dark spiral lobes, but exhibits a continuous spiral behavior near the border of the SPP. Furthermore, the pattern presents a partial azimuthal symmetry near the propagation axis, save for the area near the $+x$ axis. On the other hand, in the right columns of Figs. 12 and 15 we observe a significant difference between the phase distributions of the unapodized and the apodized SPPs, respectively, which are (1) the border vortices are no longer located on the border of the SPP, they reside on the $+x$ axis within the apodization area due to the spiraling behavior of the phase discontinuity lines beyond the border, and (2) the number of central vortices diminished considerably, now being only 1 for $\alpha=1.25$ and 2 for $\alpha=1.75$. For $\alpha=1.5$ we observe the same effects, while the chain of vortices along the $+x$ axis remains almost unscathed.

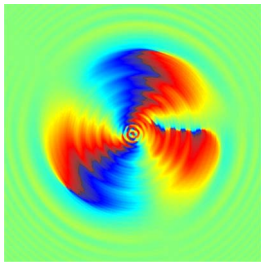

Fig. 14. (Color online) Phase distribution of the diffraction pattern observed at $z/L=2.0$, caused by a finite-radius SPP with fractional topological charge $\alpha=2.5$. We can see the chain of unit strength vortices on the $+x$ axis.

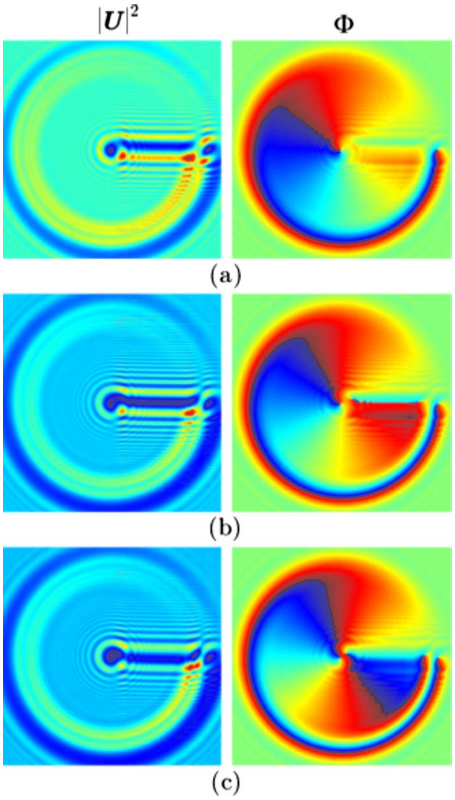

Fig. 15. (Color online) Intensity and phase of the diffraction pattern observed at $z/L=1.0$, caused by a finite-radius SPP with apodization distance $\epsilon=0.5a$ and fractional charges $\alpha=$(a) 1.25, (b) 1.5, and (c) 1.75.

5. CONCLUSIONS

In this work we studied the general problem of the finite-radius SPP with variable transmission coefficients and its modeling capabilities. We found that by setting $n=0$ and leaving a uniform phase shift $\beta\neq 0$, we could model a uniform-phase disk with variable transmission coefficients. Within the analysis of the uniform phase disk, we presented and numerically confirmed an alternate version of Babinet's principle by exploring different values of the transmission coefficients in the aperture function. We saw that the finite-radius integer-step SPP could be revised by setting $\beta=0$ and integer $\alpha=n$. We found that the finite-radius SPP has total vortex strength $S_n=0$ for all integer values of n. Furthermore, we observed that introducing phase apodization at the border of the SPP reduces the total number of vortices cointained in the diffracted wavefront, and the central vortices move closer to the propagation axis. Finally, as a more general case, we studied the finite-radius fractional-step SPP, and we observed that the integer-step case was contained within the expression for the diffraction pattern of the fractional-step SPP. We also analyzed the finite-radius fractional-

step SPP with phase apodization, and observed that the effects on the diffraction pattern are quite similar to the integer-step case, while the total vortex strength $S_\alpha = 0$ was maintained after the introduction of the phase apodization.

ACKNOWLEDGMENTS

The authors acknowledge the financial support from Consejo Nacional de Ciencia y Tecnología of México (grant 82407), and from Tecnológico de Monterrey (grant CAT141).

REFERENCES

1. M. Born and E. Wolf, *Principles of Optics*, 7th ed. (Cambridge U. Press, 1999).
2. E. Wolf and W. Marchand, "Comparison of the Kirchhoff and the Rayleigh–Sommerfeld theories of diffraction at an aperture," J. Opt. Soc. Am. **54**, 587–594 (1964).
3. W. J. Condell, "Fraunhofer diffraction from a circular annular aperture with helical phase factor," J. Opt. Soc. Am. A **2**, 206–208 (1985).
4. A. Dubra and J. A. Ferrari, "Diffracted field by an arbitrary aperture," Am. J. Phys. **67**, 87–92 (1999).
5. R. E. English, Jr. and N. George, "Diffraction from a circular aperture: on-axis field strength," Appl. Opt. **26**, 2360–2363 (1987).
6. C. J. R. Sheppard and M. Hrynevych, "Diffraction by a circular aperture: a generalization of Fresnel diffraction theory," J. Opt. Soc. Am. A **9**, 274–281 (1992).
7. C. J. R. Sheppard and M. Hrynevych, "Structure of the axial intensity minima in the Fresnel diffraction on a circular opening and superluminous effects," Opt. Commun. **271**, 316–322 (2007).
8. P. Fischer, S. E. Skelton, C. G. Leburn, C. T. Streuber, E. M. Wright, and K. Dholakia, "The dark spots of Arago," Opt. Express **15**, 11860–11873 (2007).
9. M. H. Sussman, "Fresnel diffraction with phase objects," Am. J. Phys. **30**, 44–48 (1962).
10. V. Yu. Bazhenov, M. S. Soskin, and M. V. Vasnetsov, "Screw dislocations in light wavefronts," J. Mod. Opt. **39**, 985–990 (1992).
11. M. W. Beijersbergen, R. P. C. Coerwinkel, M. Kristensen, and J. P. Woerdman, "Helical-wavefront laser beams produced with a spiral phaseplate," Opt. Commun. **112**, 321–327 (1994).
12. M. V. Berry, "Optical vortices evolving from helicoidal integer and fractional phase steps," J. Opt. A, Pure Appl. Opt. **6**, 259–268 (2004).
13. J. Leach, E. Yao, and M. J. Padgett, "Observation of the vortex structure of a non-integer vortex beam," New J. Phys. **6**, 71 (2004).
14. V. V. Kotlyar, A. A. Almazov, S. N. Khonina, V. A. Soifer, H. Elfstrom, and J. Turunen, "Generation of phase singularity through diffracting a plane or Gaussian beam by a spiral phase plate," J. Opt. Soc. Am. A **22**, 849–861 (2005).
15. V. V. Kotlyar, S. N. Khonina, A. A. Kovalev, V. A. Soifer, H. Elfstrom, and J. Turunen, "Diffraction of a plane, finite-radius wave by a spiral phase plate," Opt. Lett. **31**, 1597–1599 (2006).
16. V. V. Kotlyar, A. A. Kovalev, R. V. Skidanov, O. Y. Moiseev, and V. A. Soifer, "Diffraction of a finite-radius plane wave and a Gaussian beam by a helical axicon and a spiral phase plate," J. Opt. Soc. Am. A **24**, 1955–1964 (2007).
17. A. E. Siegman, *Lasers* (University Science Books, 1986).
18. Q. Haider and L. C. Liu, "Fourier or Bessel transformations of highly oscillatory functions," J. Phys. A **25**, 6755–6760 (1992).
19. J. C. Gutiérrez-Vega and C. López-Mariscal, "Nondiffracting vortex beams with continuous orbital angular momentum order dependence," J. Opt. A, Pure Appl. Opt. **10**, 015009 (2008).